Journal of Polymer Research (2022) 29: 118
https://doi.org/10.1007/s10965-022-02978-8

ORIGINAL PAPER

Synthesis of gum acacia-silver nanoparticles based hydrogel composites and their comparative anti-bacterial activity

Karanpreet Virk[1] · Kashma Sharma[2] · Shikha Kapil[3] · Vinod Kumar[1] · Vishal Sharma[4] · Sadanand Pandey[5] · Vijay Kumar[6,7]

Received: 5 December 2021 / Accepted: 7 March 2022 / Published online: 11 March 2022

Abstract

An interpenetrating polymer network (IPN) containing gum acacia (GA), poly(methacrylic acid) (MAA), and poly(acrylic acid) (AA) was developed using a two-step aqueous polymerization method. Firstly, semi-IPNs were produced by radical polymerization of MAA chains onto GA in the presence of ammonium persulfate as a free radical initiator and N, N′-methylene-bisacrylamide (MBA) as a cross-linking agent using a microwave heating. To obtain a semi-IPN with a higher swelling percentage, several reaction parameters such as initiator, monomer, and crosslinker concentrations were varied. The percentage swelling (%S) was highly dependent upon the reaction conditions. The optimal reaction conditions for maximal %S were 2.55×10^{-2} mol/L initiator concentration, 12 mL solvent, 0.424×10^{-3} mol/L of monomer, and 2.16×10^{-2} mol/L cross-linker concentration, according to the findings. GA-g-poly(MAA) was the name to given to the semi-IPN. Second, IPN was created by grafting AA chains onto a GA-g-poly(MAA) matrix that had been optimized. The IPN was named as a GA-g-poly(MAA-IPN-AA). The reduction of silver ions to silver nanoparticles (AgNPs) was carried out by heating the mixture of flower extract of *Koelreuteria apiculate* under microwave radiation. Finally, the as-prepared semi-IPN and IPN samples were used as templates for the loading of AgNPs. XRD, FTIR, SEM, and TGA were used to characterize the synthesized semi-IPN, IPN, and their composites with AgNPs. GA, GA-g-poly(MAA), GA-g-poly(MAA-IPN-AA), and their composites with AgNPs are tested for antibacterial activity against five common bacteria strains: *Escherichia coli*, *Micrococcus luteus*, *Pseudomonas aeruginosa*, *Rhizobium species*, and *Staphylococcus aureus*. All of the bacteria strains were shown to have a noticeable zone of inhibition when IPN and their composite with AgNPs were used. When compared to other bacteria strains, *Pseudomonas aeruginosa* was observed to be more vulnerable to the tested samples. The obtained results demonstrate that the synthesized systems are suitable for application as antibacterial agents.

Keywords Biopolymer · Silver nanoparticles · Composite hydrogels · Graft-copolymerization · Microwave irradiation · Antimicrobial properties

✉ Vishal Sharma
sharmavishal05@gmail.com

✉ Sadanand Pandey
sadanand.au@gmail.com; spandey@ynu.ac.kr

✉ Vijay Kumar
vj.physics@gmail.com

[1] Department of Applied Physics, Chandigarh University, Gharuan 140413, Punjab, India

[2] Department of Chemistry, DAV College, Sector-10, Chandigarh, India

[3] Department of Biotechnology, Chandigarh University, Gharuan 140413, Punjab, India

[4] Institute of Forensic Science & Criminology, Panjab University, Chandigarh 160014, India

[5] Department of Chemistry, College of Natural Science, Yeungnam University, 280 Daehak-Ro, Gyeongsan, Gyeongbuk 38541, Republic of Korea

[6] Department of Physics, National Institute of Technology (NIT), Hazratbal-19006, Srinagar, J&K, India

[7] Department of Physics, University of the Free State, P.O. Box 339, Bloemfontein ZA9300, South Africa

Introduction

Hydrogels are three-dimensional (3D) networks formed by the crosslinking of hydrophilic polymers [1, 2]. They might swell while maintaining their network structure by absorbing significant amounts of water or biological fluids. The inclusion of hydrophilic groups such as -OH, -CONH, -$CONH_2$, -COOH, and -SO_3H along the polymer chain contributes to their ability to absorb a large amount of water [1]. Polysaccharide hydrogel networks have received a lot of attention in recent years [3–5]. The physico-chemical properties of these hydrogels frequently differ significantly from those of the macromolecular constituents. Hydrogel characteristics can also be altered utilizing a range of physical and chemical crosslinking techniques [3, 6]. Various researchers have examined a number of polymeric systems to create hydrogels [7]. The polymer composition can be classified as natural polymeric hydrogels, synthetic polymer hydrogels, and or a combination of both [7]. Because of their non-toxicity, low cost, permeability, and biocompatibility, hydrogels have gotten a lot of attention in a variety of sectors [8–10].

Semi-interpenetrating polymer networks (semi-IPNs) and interpenetrating polymeric networks (IPNs) have developed as new materials for waste-water treatment, agricultural and horticultural applications, diapers and pad industries and biomedical and pharmaceutical applications [11–13]. The likelihood of integrating the beneficial features of each polymeric constituent of IPNs or semi-IPNs, resulting in a novel system with qualities that differ from the two separate components, has piqued interest in these structures [12, 14]. Semi-IPNs or IPNs develops the possibilities to tailor the features of the subsequent materials via selecting accurately the initial components of the IPN and semi-IPN frameworks [12]. Natural polysaccharides are used as a popular material for the synthesis of semi-IPN and IPNs hydrogels due to their favourable polymer system, abundance in nature, biocompatibility, and the likelihood to change their chemical structure through simple and efficient reactions [12, 15].

Gum acacia (GA) is a non-cytotoxic, hemostatic, nonhemolytic, antibacterial, antioxidant, biocompatible, cost-effective and anti-inflammatory natural polysaccharide [16–18]. GA is extracted from the stems and branches of *Acacia Senegal* trees, and its chemical composition varied depending on the tree's age, climate, and local soil conditions [19, 20]. It is normally composed of D-galactose, L-arabinose, L-rhamnose, D-glucuronic acid, and 4-O-methylglucuronic acid units which are joined by β-glycosidic chains [16–18]. In 2015, the potential applications of natural polymer GA were studied [21]. Several authors have described the synthesis of stimuli-responsive hydrogels based on GA [16, 22, 23].

Silver (Ag) is well-known for its antimicrobial and disinfectant properties, and it has a wide range of uses in medication and pharmaceutics [24–26]. While silver nanoparticles (AgNPs) are gaining a lot of attention due to their ability to discharge Ag particles in a controlled way, which has a tremendous antibacterial effect on a wide range of microscopic organisms. AgNPs can agglomerate into groups due to their high surface to volume ratio, which limits their application. AgNPs in graft copolymeric systems represent a promising solution for stability and dispersal issues [27–29]. Furthermore, incorporating AgNPs into semi-IPN and IPN matrices based on GA can result in new composite hydrogels with improved antimicrobial properties. Because of their superior permeation and retention capabilities, AgNPs have been found to be particularly effective as an antibacterial agent, both in vivo and in vitro, when compared to bulk silver [20, 29, 30].

Zakia et al. [31] described a straightforward method for making alginate and AgNP hydrogels, as well as their antibacterial efficacy against a model bacterium (E. coli). They used a photo-crosslinking approach after changing the chemical structure of the polymer backbone with a methacrylate group to achieve homogeneous AgNP dispersion in the hydrogel. Mohan et al. [32] developed antibacterial hydrogel–silver nanocomposites that can be used in a variety of medical applications. Their research shows that hydrogels can be used as templates to create metal nanostructures of various sizes and morphologies. The composition of monomers or semi-IPN polymer chains, as well as the degree of cross-linking, appear to be important determinants in determining the shape and size of nanoparticles. Varaprasad et al. [33] developed poly(acrylamide)/poly(vinyl alcohol) hydrogel–silver nanocomposites to produce AgNPs with a size of 2–3 nm in gel networks. The production of nanocomposite is simple, direct, and quick, and the resulting hydrogel AgNP composites can be employed for antibacterial and wound dressing applications. Dai et al. [34] established a novel paradigm for the manufacture of silver nanoparticles (AgNPs)-containing smart hydrogels using guar gum and sodium borohydride ($NaBH_4$) in a simple, rapid, and cost-effective manner. They concluded that their study indicates a new class of smart metal nanoparticles/natural polymer-based hydrogels that can be made in a single step with $NaBH_4$. Juby et al. [20] described a one-pot synthesis of AgNPs within a polyvinyl alcohol/GA hydrogel via gamma irradiation-induced crosslinking. They discovered that adding GA to the hydrogels improved their biocompatibility and swelling properties. Against gram-negative *E. coli* bacteria, the composites demonstrate significant antibacterial activity. Singh and Dhiman [35] used GA-carbopol-crosslinked polyvinylimidazole hydrogels to wound dressings for the delivery of antibiotics and anaesthetics. Li et al. [36] developed a chronic wound healing delivery vehicle based on bioinspired alginate-gum Arabic hydrogels. GA extract has been shown to be haemostatic, non-haemolytic, and antimicrobial in recent research [37, 38].

We previously demonstrated the production of antibacterial and antifungal gum-acacia-poly(acrylamide-IPN-acrylic acid) nanocomposite hydrogels loaded with AgNPs [39]. In view of the same, it was planned to use microwave radiation to prepare GA-g-poly(MAA) and GA-g-poly(MAA-IPN-AA) hydrogels using a two-step aqueous free radical polymerization method. For the loading of AgNPs, the semi-IPN and IPN samples were employed as templates. These composite network systems provide state-of-the-art, with one portion of the polymeric network tries to improve the percentage swelling while another anchors antimicrobial characteristics. This opens a new window to tailor the property of interest. FTIR, SEM–EDX, XRD, and TGA were used to characterise the resulting semi-IPN, IPN, and their composites with AgNPs. Five strains *Escherichia coli (E. coli)*, *Micrococcus luteus (M. luteus)*, *Pseudomonas aeruginosa (P. aeruginosa)*, *Rhizobium species (R. species)*, *Staphylococcus aureus (S. aureus)* were used to test antibacterial properties in vitro. The main purpose was to evaluate the efficacy and antibacterial capabilities of the hydrogels and composites developed against a variety of bacteria available in our lab.

Materials and methods

Materials

Gum acacia (GA) was procured from Sisco Research Laboratories Pvt. Ltd (India). Ammonium persulfate (APS) was procured from Sigma Aldrich (USA). The monomer methacrylic acid (MAA) and acrylic acid (AA) were procured from LOBA CHEMIE PVT Ltd (India). The cross-linker N,N' methylene bisacrylamide (MBA) was procured from Central Drug House Ltd (India). On the other hand, $AgNO_3$ was procured from Merck, India. Distilled water was used during the synthesis process. The preparation of semi-IPN and IPN hydrogels was carried out in microwave equipment (IFB 20L) at 2450 MHz and 1200 W (India). The time for the synthesis of samples and microwave power @ 20% of the microwave oven remains the same throughout the synthesis procedure.

Preparation of semi-IPN and IPN hydrogels

Hydrogel based on GA was synthesized using microwave radiation with MAA as a monomer, APS as initiator, distilled water as a solvent, and MBA as a crosslinker. The microwave oven 17PM-MECI (IFB) utilised in the synthesis runs on 230 V- 50 Hz and operates at a frequency of 2450 MHz. 0.5 g of GA was weighed and mixed with a known amount of dH2O in the experiment. A known amount of APS was added to this, followed by MAA and MBA, and the solution was continually stirred in a clockwise orientation. To get the hydrogel with the best percentage swelling (%*S*), several reaction parameters such as initiator, cross-linker, and monomer concentrations, as well as the amount of solvent, were changed. Microwave irradiation was used for 40 s on the mixture. The synthesised hydrogel was given a repeated washing by soaking it in 10 ml distilled water for about 10 min and then drying it in a hot air oven at 60 °C. By weighing the hydrogels before and after swelling, the degree of swelling was determined gravimetrically. The conventional formulas were used to calculate the percentage swelling (%*S*) and grafting percentage (%*G*) of the produced hydrogels:

$$\textit{Percentage swelling } (\%S) = \frac{W_t - W_o}{W_o}$$

where, W_t is the weight of polymer sample after swelling and W_o is its initial weight of in dry state.

$$\%G = \frac{W_f - W_b}{W_b} \times 100$$

where, W_f is the weight of functional polymer, and W_b is the weight of formed dried backbone.

GA-g-poly(MAA-IPN-AA) IPN hydrogels were prepared using preoptimized parameters used for the development of semi-IPN hydrogel under microwave radiation. A known amount of AA monomer was added drop-by-drop in optimal semi-IPN and distilled water in the experiment, and the mixture was continuously stirred. Continuous stirring was used to add the pre-optimized MBA. Optimized concentrations of APS (initiator) and MBA (cross-linker) were added to this reaction mixture. The reaction mixture was kept at room temperature for 14 h, which resulted in the formation of swollen hydrogels. Following that, the reaction mixture was agitated for a few minutes before being microwaved for two minutes to create IPN hydrogel. The IPN hydrogels were also rinsed many times with distilled water to remove homopolymers before being dried at 60 °C in a hot air oven. Table 1 displays the findings of the optimum %*S* and %*G*.

Preparation of silver nanoparticles (AgNPs)

By heating a mixture of flower extract of Koelreuteria apiculate under microwave radiation, silver ions were reduced to AgNPs. Our previous work [39] describes the full synthesis technique for the preparation of AgNPs.

Table 1 Optimum reaction conditions affording maximum percentage swelling for synthesis of GA-g-poly (MAA) and GA-g-poly(MAA-IPN-AA)

Sample Code	Optimized reaction parameters								%G	%S
	Back-bone (g)	Initiator (mol/L) $\times 10^{-2}$	Time (min.)	Amt. of solvent (ml)	pH	Monomer (mol/L) $\times 10^{-3}$	Cross-linker (mol/L) $\times 10^{-2}$	MW Power (%)		
GA-g-poly(MAA)	0.5	2.55	4	12	7	0.424	2.70	20	282	588
GA-g-poly(MAA-IPN-AA)	0.5	2.55	2.16	12	7	0.612	2.70	100	350	500

Synthesis of composite hydrogels

The ex-situ approach was used to prepare composite samples, as described in our previous work [39]. The loading of previously prepared AgNPs into the hydrogel matrices was completed by dipping 2 g of preoptimized poly(MAA) and GA-g-poly(MAA-IPN-AA) in 60 ml of AgNPs solution for 24 h each, and then placing the samples in a hot air oven at 60 °C for 24 h to achieve the preferred composites.

Characterizations

An FTIR spectrophotometer (Perkin Elmer) with diamond crystal and ZnSe for the focusing element was used to characterise the synthesised samples. SEM was used to determine the surface morphology of the composites (JEOL JSM-6490LV). Before the measurement, the samples were dried in air and sputter-coated with gold. The confirmation of AgNPs in the semi-IPN and IPN samples were confirmed by using EDX spectra. XRD pattern was measured by employing a Spinner PW3064, X'pert PRO diffractometer with Cu-K_α of 0.154056 nm at the 2θ scale. The thermal stability of prepared hydrogels was studied using a Thermal Analyzer (STA) STA7200.

In vitro microbiological assessment

The antibacterial properties of GA, GA-g-poly(MAA), GA-g-poly(MAA-IPN-AA), and their composites with AgNPs were tested using the agar well-diffusion method. For test organisms, MHA (Mueller Hinton Agar) was utilised as a supportive culture medium [40, 41]. The test organisms for the experiment (OD ≤ 0.1 at 600 nm) were gram-positive (*S. aureus* and *M. luteus*) and gram-negative (*Rhizobium species*, *E. coli*, and *P. aeruginosa*) bacterial cultures that had been cultivated overnight. A 50 mg sample of each of the test samples was used. In the assay, an antibiotic (Norfloxacin 5mcg) was employed as a control, and the zone of inhibition was determined in millimetres. The MHA plate surface is incubated by using a sterile cotton swab to disperse the necessary amount (100 µl) of the test organism (OD ≤ 0.1 at 600 nm) across the entire agar surface. Then, using a sterile cork borer or an autopipette tip, a well with a diameter of 6-8 mm is punched aseptically (1 mL). The necessary amount of test sample (50 mg) is aseptically injected into the well, and the assay plates are carefully transferred to an incubator (37 °C) for overnight incubation. The test sample diffuses in the agar media and inhibits the test organism's growth, as assessed by the zone of inhibition.

Results and discussion

Reaction mechanism

The probable crosslinking mechanism is depicted in Scheme 1 and consists of three steps: chain initiation, chain propagation, and chain termination. These reactions are well known in the literature. Under the action of microwave heating, ammonium persulfate may break down to peroxodisulfate ions [$(S_2O_8)^{2-}$], and subsequent removal of electrons from $(S_2O_8)^{2-}$ results in the creation of sulphate ions [42]. Continuous microwave heating can produce sulphate ion radicals ($SO4^{*-}$), which combine with H_2O molecules to create hydroxyl radicals (OH^*) [42, 43]. The –OH groups of the GA backbone and methacrylic acid (MAA) monomer chains are attacked by these free radicals (SO_4^{*-} and OH^*), resulting in the formation of macro radicals for the reaction. At the active sites, the stimulated MAA chains were grafted into the GA backbone to create a partially cross-linked network. To make GA-g-poly(MAA) semi-IPN hydrogels, MBA was used to cross-link the poly(MAA) and partially grafted network. The production of covalent bonds results from the recombination of macro radicals on various chains, followed by the construction of a cross-linked network [44]. AA monomer units were grafted onto GA-g-poly(MAA) semi-IPN hydrogel in a similar way. Due to the presence of SO_4^{*-} and OH^* radicals in the reaction mixture, active sites were produced on the AA monomer and semi-IPN hydrogel. IPN GA-g-poly(MAA-IPN-AA) hydrogel is the name given to the resulting network.

Scheme 1 Mechanism of graft copolymerization of methacrylic acid onto gum acacia

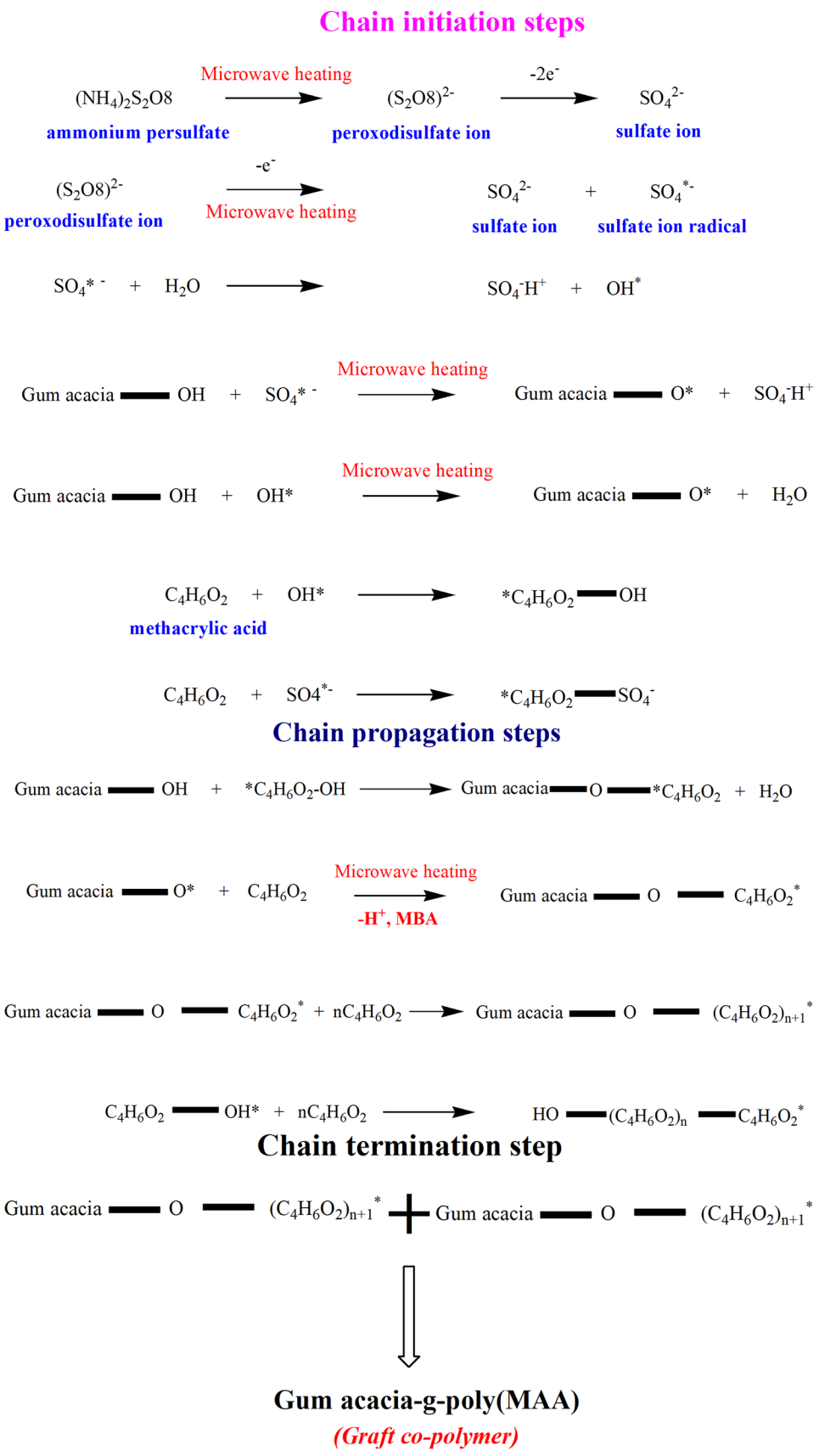

Optimized reaction conditions

The concentration of the initiator, the amount of solvent, the reaction time, the monomer concentration, and the crosslinker concentration were all optimized (Table 1). The degree of grafting and swelling capacity of hydrogels are heavily influenced by these parameters. Various reaction conditions influencing percentage swelling (%*S*) and percentage grafting (%*G*) are discussed below:

The initiator concentration was varied from 0.0182–0.0328 mol/L to study its effect on percentage swelling (Fig. 1a). The %*S* is improved with increasing initiator concentration. This is expected behavior in hydrogel networks that has been explored earlier by various authors [45, 46]. The %*S* attained a maximum value at the initiator concentration of 0.0255 mol/L. After this, the %*S* decreased with a further increase in initiator concentration. At lower concentrations, the rise in %*S* is ascribed to the rise in the number of free radicals generated on.

The amount of the solvent was varied from 6 ml – 14 ml and its effects on the %*S* are shown in the (Fig. 1b). The increase in %*S* was observed until 12 ml of the solvent concentration and after it decreased [47]. The optimized amount of the solvent was identified to be 12 ml for attaining maximum %*S*. This may be owing to the fact that at the optimum amount of solvent there is a generation of hydroxyl radical ions giving more active sites for polymerization and thus gives rise in %*S*. Above the optimized amount of solvent, the %*S* started decreasing due to the lack of active sites for graft polymerization over the GA backbone and on monomer [48].

The changes in percentage swelling (Fig. 1c) was also studied by varying the monomer concentration. The %*S* increased with a rise in the concentration of monomer achieving maximum %*S* at 0.424×10^{-3} mol/L concentration

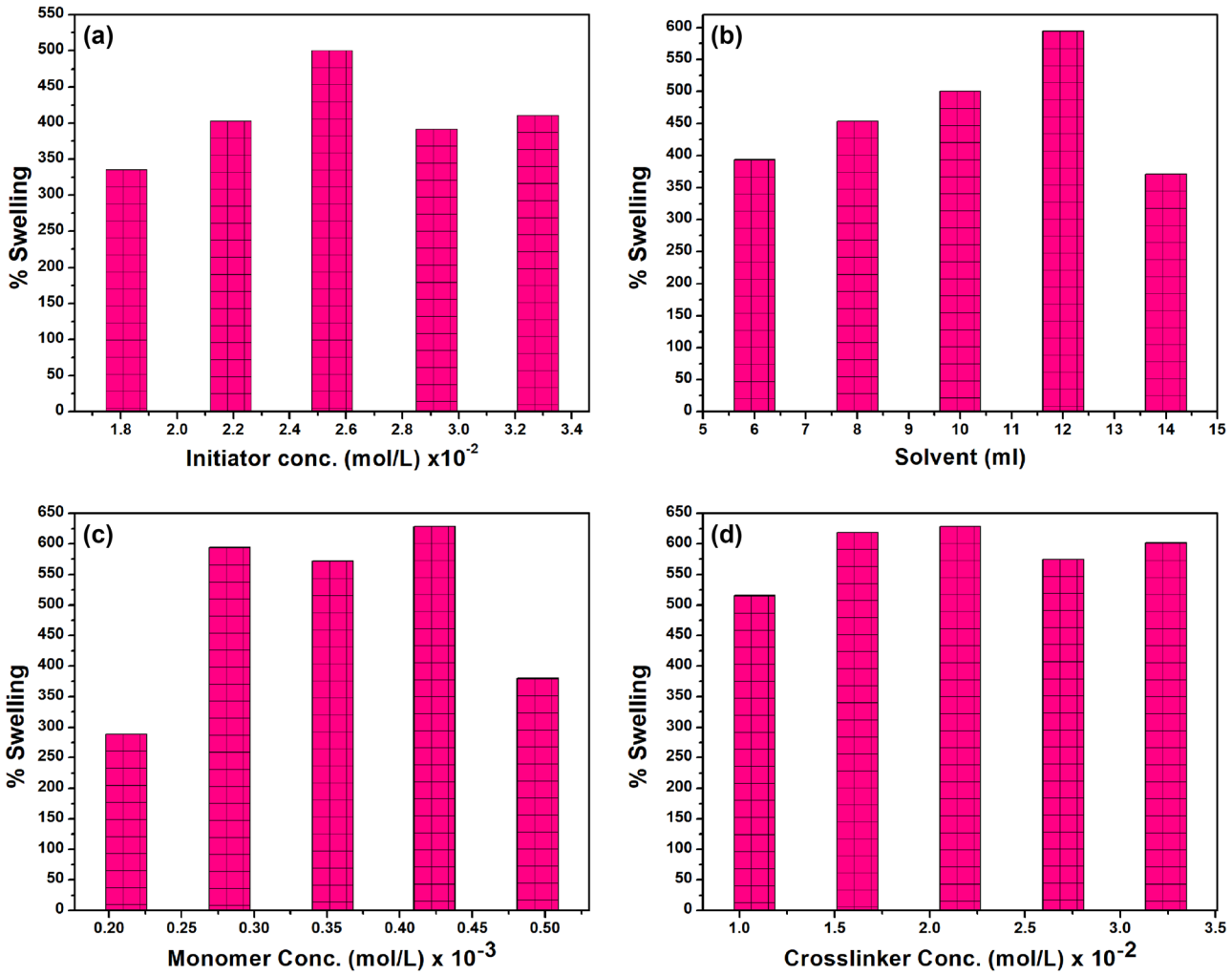

Fig. 1 Variation of percentage swelling with (**a**) initiator concentration, (**b**) amount of solvent, (**c**) monomer concentration, and (**d**) crosslinker concentration

of MAA and later it decreased. This behavior arises from the fact that in initial stages greater availability of hydrophilic monomer MAA for its cross-linking with GA backbone thus increasing the affinity of water absorption resulting in high %*S*. However, above the optimized MAA concentration the %*S* decreased because of the increased viscosity of the solution that hindered the motion of free radicals and monomer molecules and by the virtue of preferential homo polymerization than graft copolymerization [49].

The concentration of cross-linker was varied from 0.0108–0.0324 mol/L to study its effect on %*S* (Fig. 1d). The crosslinker is necessary as it makes the hydrogel insoluble in water by completely dissolving the hydrophilic polymer chains into an aqueous solution [49]. The %*S* increased by the rise in the concentration of MBA till 0.0216 mol/L where the maximum %*S* of 628% was achieved. On the basis of Flory's network theory, the fluid absorbency in hydrogels, and the density of cross-linking is determined from the concentration of the cross-linking chain [50]. Therefore, the number of network chains enhanced with a rise in the concentration of cross-linker resulting in an improved density of cross-linking. With the rise in MBA content above 0.0216 mol/L, the swelling capacity of grafted polymer decreased. It is because with increased cross-linker concentration there may be a generation of many chains in the polymeric network resulting in a highly compact and rigid structure. This suggested structure would result in low swelling as it will not succeed to uptake a large volume of water.

FTIR spectra analysis

To confirm the graft copolymerization mechanism, FTIR spectroscopy was used. Figure 2 shows the FTIR spectra of GA, semi-IPN, IPN, semi-IPN-AgNPs and IPN-AgNPs. The GA exhibited a broad peak at 3285 cm^{-1}, which is attributed to the hydrogen-bonded OH group [39]. No wide peak is found in any of the samples after grafting in the range 3300–3500 cm^{-1}, which indicates the stability of all the samples. The peak at 2925 cm^{-1} and 2990 cm^{-1} in all the samples is ascribed due to the C-H stretching. However, these peaks are quite prominent in semi-IPN-AgNPs and IPN. The slight shift in peak positions and variations in peak intensity indicates the impregnation of AgNPs onto the hydrogel matrices based on semi-IPN and IPN hydrogels. The sharp peaks around 1696 cm^{-1} and 1157 cm^{-1} attributed due to –C = O stretching of carbonyl groups and C–O stretching, respectively [45]. The small peaks in the range of 1030–1070 cm^{-1} is arises due to the stretching vibration of C–O–C and C–O–H bonds, which confirms the saccharide structure of the prepared composite samples [45]. The peak at 1258 cm^{-1} attributed to C–N stretching vibrations [43]. It is clear from Fig. 2 that the wavenumber of prepared hydrogels is slightly shifted after

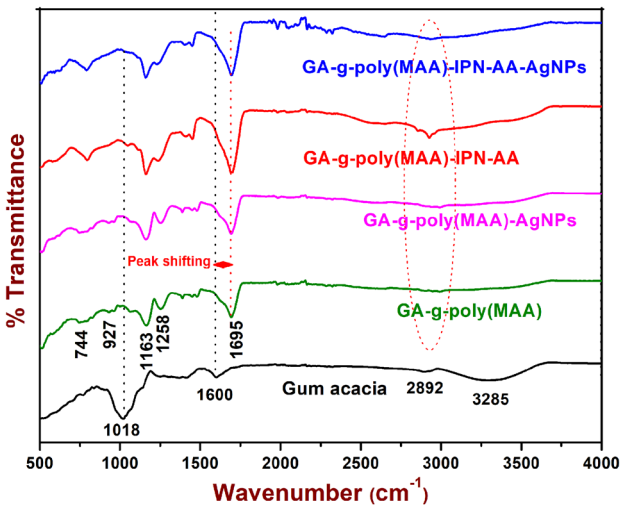

Fig. 2 FTIR spectra of semi-IPN, IPN and their nanocomposites with silver nanoparticles

incorporation of AgNPs towards higher or lower wavenumber region which indicated the creation of covalent bonding among AgNPs and electron-rich units of the GA-g-poly(MAA) and GA-g-poly(MAA-IPN-AA) hydrogels. The observed peak shows network chain formation due to polymerization of MAA and on GA and further polymerization of AA on the GA-g-poly(MAA) network. Results of FTIR studies reflected the presence of GA, MAA, and AA in the semi-IPN and IPN hydrogels.

SEM–EDS analysis

SEM was used to analyse the surface morphology of the synthesized hydrogel systems and their composites with AgNPs, and the resulting micrographs are shown in Fig. 3. GA exhibits a uniformly homogeneous surface morphology (Fig. 3a) [39]. The surface morphology of the resultant semi-IPN is entirely modified after graft copolymerization with MAA. A rough surface with a honey beehive-like structure may be seen in the microscope (Fig. 3b). Further crosslinking with AA resulted in IPNs with a visible uniform crossing fiber-like shape, which increases roughness and agrees well with XRD results (Fig. 3c). Alternatively, the incorporation of AgNPs into the IPN matrix shows a clear formation of IPN AgNPs composite. The roughness is increased and visible globular knots are appeared over highly crisscrossed fibers like geometry (Fig. 3d).

The elemental analysis of AgNPs loaded semi-IPN and IPN composite was done by using EDS to confirm the incorporation of AgNPs in the hydrogel networks (Fig. 4). The presence of Ag peaks show that AgNPs are incorporated into the semi-IPN and IPN matrix.

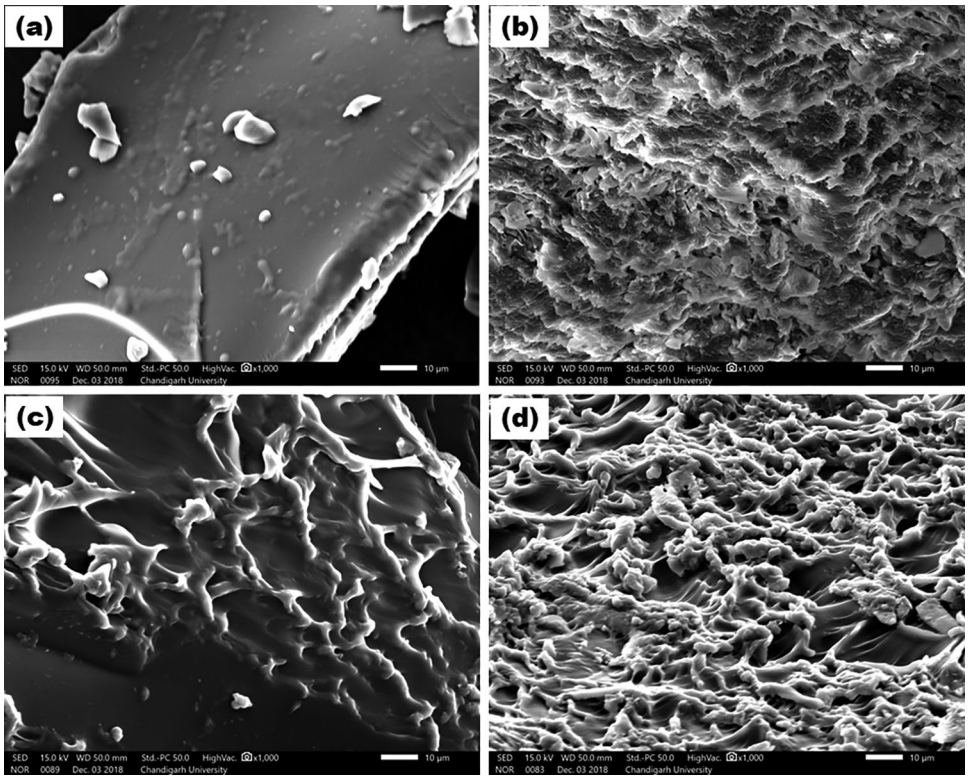

Fig. 3 SEM images (**a**) Gum acacia, (**b**) semi-IPN, (**c**) IPN, and (**d**) IPN-AgNPs nanocomposite

XRD analysis

The XRD patterns of GA, semi-IPN, IPN, semi-IPN-AgNPs, and IPN-AgNPs are displayed in Fig. 5. In GA a broad peak at around 19° was obtained at 2θ scale with a comparatively lesser intensity in contrast to the prepared hydrogels [38]. The diffraction pattern of GA is semi-crystalline with a dominant amorphous nature. The crosslinking of GA with MAA showed that the broad maxima shifted towards a higher angle and another sharp peak is obtained at an angle 15.6°. The crosslinking of MAA chains onto GA increases the relative intensity which suggested the improvement of crystallinity due to the interaction of MAA chains with different groups GA backbone [39]. In the case of AgNPs loaded semi-IPN, similar behaviour is observed with a small drop in peak intensity.

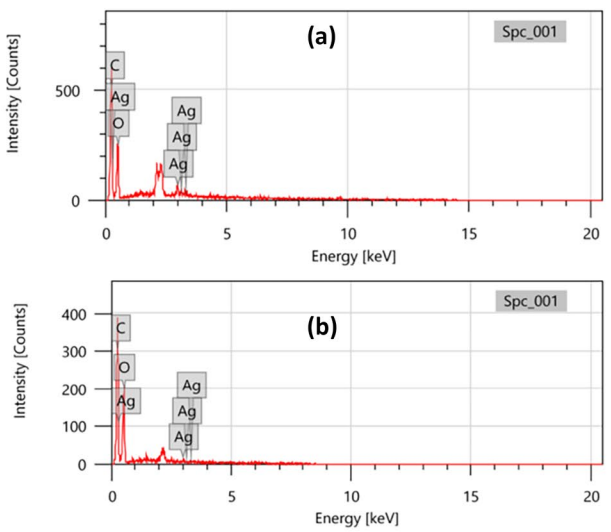

Display name	Standard data	Quantification method	Result Type
Spc_001	Standardless	ZAF	Metal

Element	Line	Mass%	Atom%
C	K	43.41±0.38	54.39±0.48
O	K	47.07±1.06	44.28±1.00
Ag	L	9.52±0.63	1.33±0.09
Total		100.00	100.00
Spc_001			Fitting ratio 0.5357

Display name	Standard data	Quantification method	Result Type
Spc_001	Standardless	ZAF	Metal

Element	Line	Mass%	Atom%
C	K	47.25±0.52	56.22±0.62
O	K	48.36±1.28	43.20±1.14
Ag	L	4.39±0.99	0.58±0.13
Total		100.00	100.00
Spc_001			Fitting ratio 0.4676

Fig. 4 EDS spectra of (**a**) semi-IPN-AgNPs and (**b**) IPN-AgNPs

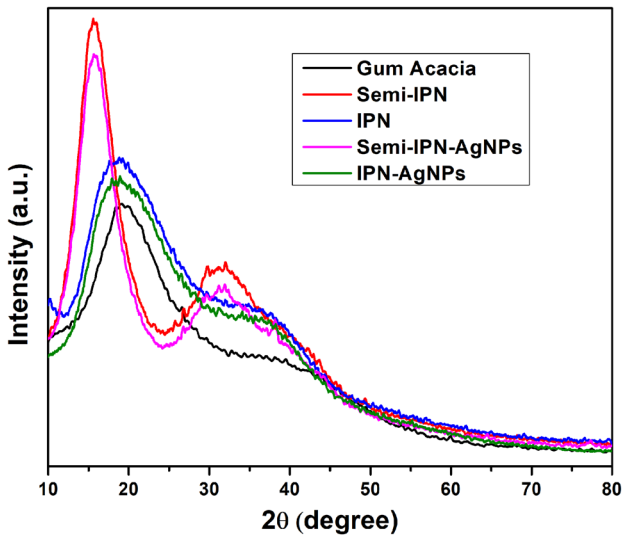

Fig. 5 XRD patterns of semi-IPN, IPN and their nanocomposites with silver nanoparticles

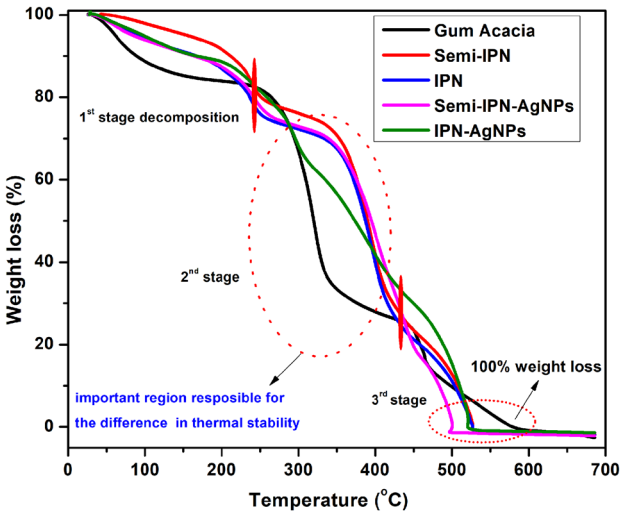

Fig. 6 TGA spectra of gum acacia, semi-IPN, IPN and their nanocomposites with silver nanoparticles

The observed changes in peak intensity point out the interaction of Ag ions in the semi-IPN matrix, which shows the transformation of the semi-IPN network to the amorphous system. Furthermore, adding AA to the synthesized semi-IPN matrix causes a slight shift in the intensity of diffraction peak. The loading of AgNPs into the IPN matrix, on the other hand, exhibits the same behavior, while the intensity of the diffraction peak decreases slightly. These findings are in line with the results of the SEM.

TGA analysis

The thermal behaviour of the backbone, semi-IPN, IPN, and composite with AgNPs was investigated using thermal analysis. The various degradation stages of the hydrogels and their composites with AgNPs are depicted in Fig. 6. Table 2 shows the corresponding weight loss at various temperatures. Initially, the GA shows maximum and frequent weight loss in each step as compared to its cross-linked structure. This mass loss is credited to the loss of the hydroxyl group of GA as a water molecule that leads to a fast decomposition of the backbone. The TGA spectrum of GA-g-poly(MAA) and GA-g-poly(MAA-IPN-AA) showed good thermal stability. Initial weight loss of 20–25% in both semi-IPN and IPN at the range 250 °C is attributed to the removal of free water and unreacted monomers from the hydrogels network. The 2nd stage weight loss of 25–60% from 300 °C to 400 oC was due to the removal of loosely bounded water from polymer network and breakage of physical forces involved in the hydrogel formation [35]. The last stage weight loss of 60–90% from 400 °C to 600 °C was due to complete thermal destruction of carboxylic groups, breakage of covalent bonds, splitting of backbone, and disruption of cross-linking of polymer networks [16, 43]. As expected, the thermal stability of IPN was further improved when loaded with the AgNPs as only 60–75% weight loss was only observed between 400 °C to 500 °C. Similar findings were reported by various authors [35, 51]. The improved thermal stability of the AgNPs incorporated semi-IPN and IPN may be because of two possible reasons [20]. Firstly, it is a well-known fact that AgNPs have higher thermal stability as compared to polymeric systems. Subsequently, the incorporation of AgNPs in the hydrogel matrix improves the thermal behaviour of the hydrogels. Secondly, more stability could be due to decreased mobility of the hydrogel chains on the impregnation of AgNPs. The AgNPs interact with poly(AA), poly(MAA) and GA through the -COOH and -OH groups present in the semi-IPN and IPN, as also clear by the outcomes of the FTIR spectra. This type of interaction causes weak intermolecular cross-linking between AgNPs and semi-IPN and IPN. Therefore, the degradation process can be slow down at lower temperatures, but it can be quick at higher temperatures after the AgNPs have been loaded [52]. The TGA results demonstrate that the synthesized hydrogel and their nanocomposites with AgNPs are more thermally stable.

In vitro antimicrobial studies

By using the agar well diffusion method, the antibacterial potential of GA, GA-g-poly(MAA), GA-g-poly(MAA-IPN-AA) and hydrogel composites with loaded AgNPs against *E. coli* (Gram-negative), *M. luteus* (Gram-positive) *P. aeruginosa* (Gram-negative), *R. species* (Gram-negative) and *S. aureus* (Gram-positive) bacteria was investigated

Table 2 Thermal analysis data of GA and crosslinked hydrogels

Sample name	Weight loss (%) at different temperature					
	250 °C	**300 °C**	**350 °C**	**400 °C**	**450 °C**	**500 °C**
GA	18	33	67	73	77	90
Semi-IPN	20	24	29	59	73	87
Semi-IPN-AgNPs	23	27	32	53	81	99
IPN	24	28	33	59	79	89
IPN-AgNPs	19	32	44	58	70	75

(Fig. 7). The inhibition zone diameter was measured in millimetres and is listed in Table 3. *M. luteus* is gram-positive bacteria that can be found in mucous membranes, water, and soil [53, 54]. This bacterium causes infections like septic shock and arthritis, endocarditis, meningitis, and cavitary pneumonia in immunosuppressed patients [54]. *E. coli* is well-known gram-negative bacterium remains present in aerobic commensal inhabitant of the large intestine and certain strains of E. coli. cause diarrhea, and urinary tract infections [55]. *R species* is gram-positive bacteria that is responsible for nitrogen fixation in leguminous plants [56]. Rhizobium has identified as the main contaminant of DNA extraction kit reagents and ultrapure water systems. *P. aeruginosa* is a Gram-negative, rod-shaped, asporogenous, and monoflagellated bacterium that causes plant and animal disease [57]. It causes severe infections in immunocompromised cancer patients and patients suffering from severe burns [57]. *S. aureus* is a major human pathogen causing multiple clinical infections like bacteremia and infective endocarditis, osteoarticular, skin and soft tissue infections, and pleuropulmonary [58]. The zone of bacterial growth inhibition was found to be 14 ± 0.5 mm, no inhibition, 16 ± 0.5 mm, 11 ± 0.5 mm and no inhibition against *E. coli*, *M. luteus*, *P. aeruginosa*, *R. species* and *S. aureus* with semi-IPN. In the case of AgNPs loaded semi-IPN composite, the zone of bacterial growth inhibition was bigger with a diameter of 16 ± 0.5 mm, inactive, 18 ± 0.5 mm, 13 ± 0.5 mm and 14 ± 0.5 mm against *E. coli*, *M. luteus*, *P. aeruginosa*, *R. species*, and *S. aureus* respectively. The zone of inhibition in case of IPN was found to be 20 ± 0.5 mm, 14 ± 0.5, 23 ± 0.5, 16 ± 0.5 mm, and 14 ± 0.5 mm against *E. coli*, *M. luteus*, *P. aeruginosa*, *R. species* and *S. aureus*, respectively. In case of AgNPs loaded IPN composite, the zone of bacterial growth inhibition was found to be more prominent and expanded i.e. 21 ± 0.5 mm, 13 ± 0.5, 25 ± 0.5, 17 ± 0.5 mm and 16 ± 0.5 mm against *E. coli*, *M. luteus*, *P. aeruginosa*, *R. species* and *S. aureus*, respectively. As can be seen from Fig. 6 and Table 3, after 24 h of incubation at 37 °C, all four types of samples showed an antibacterial effect on all the bacteria. The GA backbone shows antibacterial activity against *E. Coli* (11 ± 0.5), *P. aeruginosa* (8 ± 0.5) and *R. species* (8 ± 0.5). GA contains chiefly arabin, a mixture of calcium, magnesium, and potassium salts of Arabic acid [19]. The Arabic acid on hydrolysis produces Lrhamnopyranose, Larabofuranose, galactopyranose, and taldobionic acid 6-dglucuronosido-d-galactose. The gum has also contained enzymes like oxidases, peroxidases, and pectinases. GA boosts the antimicrobial activities due to the presence of these bioactive agents like tannins, oxidases, peroxidases, pectinases, alkaloids, cardiac glycosides, flavonoids, volatile oils, saponins, and anthraquinone. The semi-IPN and IPN show excellent antibacterial activity against + ve and –ve strains.

The possible mechanism is explained in Scheme 2. The resulting semi-IPN and IPN produced charged hydrogels having stereo complexation and these complexes give strong fiber-like morphology as confirmed by SEM images that significantly enhanced antimicrobial activity against both Gram-positive/Gram-negative bacteria through interfacial stereochemistry [59, 60]. The antimicrobial mechanism involves lysis of cell walls by a blockage in the biosynthesis of peptidoglycan, making bacterial cells more susceptible to osmotic lysis. The GA and acrylates present in the hydrogels interfere with the nucleic acid metabolism, protein synthesis, and repair of bacterial cells leading to bactericidal effect. The cellular contents of both + ve and –ve bacterium, which is surrounded by an inner peptidoglycan cell wall as well an inner plasma membrane. Gram-negative bacteria possess outer lipid bilayer. The semi-IPN and IPN block the biosynthesis of the cell wall through weakening the peptidoglycan and compromising the structural integrity that causes disruption of bacterial cells [61, 62].

The incorporation of AgNPs to semi-IPN and IPN resulting in a composite having enhanced antibacterial activities against all five types of + ve and –ve bacterial strains. The AgNPs showed good dispersion ability throughout the hydrogel network. The bactericidal properties of AgNPs against bacteria have been a well-known fact for centuries. The Ag^+ ion can easily bind to the bacterial cell membrane due to its small size [63, 64]. This creates interaction between Ag^+ and thiol group of proteins on the bacterial cell membrane [25]. Hence, disturbing the bacterial cell's viability by obstructing the replication of DNA [64, 65]. AgNPs get easily diffused through bacterial cell membranes cause hindrance in the functions of respiratory

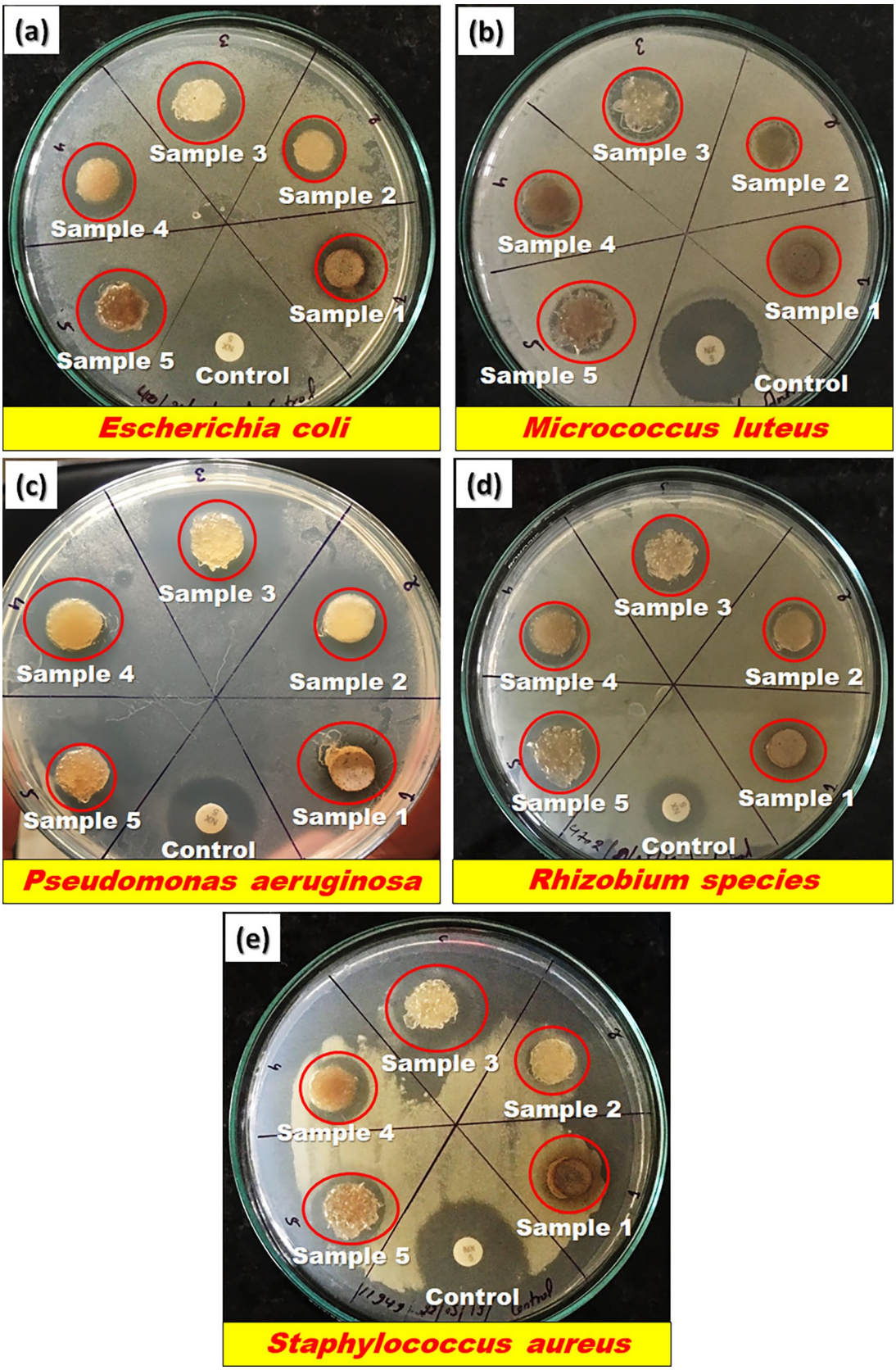

Fig. 7 Antimicrobial activities of the prepared samples with various bacterial strains

Table 3 Antibacterial activity of synthesized hydrogels against bacterium *Escherichia coli, Micrococcus luteus, Pseudomonas aeruginosa, Rhizobium species* and *Staphylococcus aureus*

S. No	Name of Bacteria	Inhibition zone diameter (mm)				
		Gum Acacia	Semi-IPN	IPN	Semi-IPN-AgNPs	IPN-AgNPs
1	*Escherichia coli (Gram-negative)*	11 ± 0.5	14 ± 0.5	20 ± 0.5	16 ± 0.5	21 ± 0.5
2	*Micrococcus luteus (Gram-positive)*	0 (inactive)	0 (inactive)	14 ± 0.5	0 (inactive)	13 ± 0.5
3	*Pseudomonas aeruginosa (Gram-positive)*	8 ± 0.5	16 ± 0.5	23 ± 0.5	18 ± 0.5	25 ± 0.5
4	*Rhizobium species (Gram-negative)*	8 ± 0.5	11 ± 0.5	16 ± 0.5	13 ± 0.5	17 ± 0.5
5	*Staphylococcus aureus (Gram-positive)*	0 (inactive)	0 (inactive)	14 ± 0.5	14 ± 0.5	16 ± 0.5

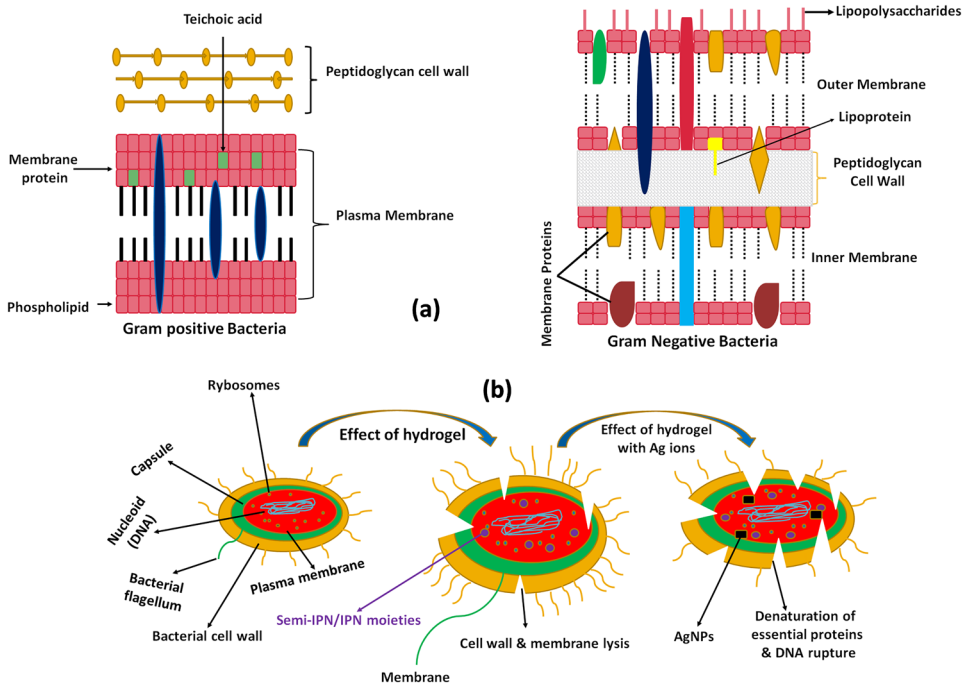

Scheme 2 Probable mechanism of antibacterial activity (**a**) cell membrane of gram positive and gram negative bacteria, (**b**) lysis of the cell membrane through its interaction with hydrogels and AgNPs

Table 4 Comparison of antibacterial activity of natural polysaccharide based hydrogels against various bacteria

S. No	Hydrogels	Bacteria	Inhibition Zone	References
1	Polyvinyl alcohol/gum karaya/ silver nanoparticles	*E. coli*	14.0	[69]
		P. aeruginosa	14.5	
		S. aureus	14.5	
2	Guar Gum-2/curcumin-AgNPs 3.14 nM hydrogel	*E.coli*	13.5	[70]
		P. aeruginosa	13.0	
		S.aureus	15.0	
3	PVA-GG hydrogels with 4 µg/mL AgNPs	*E. Coli*	11.5	[71]
4	Guar gum/P70) containing cinnamaldehyde-loaded chitosan nanoparticles	*S. aureus*	14.3 ± 1.12	[72]
5	PVA/PANI/Ag nanocomposites (at 15% AgNPs)	*E. coli*	12	[73]
		Staph. aureus	15	
6	Bacterial cellulose/silver nanocomposite hydrogels	*S. aureus*	26 ± 0.35	[74]
		E. coli	28 ± 0.16	

chain proteins and transport proteins [66]. The AgNPs even in small concentrations produces excess proton leakage throughout bacterial cell membranes causing loss of proton motive force [67]. The interaction of AgNPs with the dissolved oxygen produced reactive oxygen species that resulted in oxidative stress and free radical attacks onto the membrane lipids leads to the breakdown of the cell membrane that results in final death of bacteria [66, 68]. Table 4 compares the antibacterial activity of similar hydrogels systems against various bacteria.

Conclusion

Antimicrobial materials have been studied extensively in response to rising microbial resistance to traditional antibiotics and disinfectants. Natural polysaccharide-based hydrogels and their composites containing metal nanoparticles could be suitable for antibacterial applications in some cases. Using a microwave irradiation approach, we were able to successfully synthesis GA-g-poly(MAA) and GA-g-poly(MAA-IPN-AA) based hydrogels from GA. APS and MBA being used as initiator and cross-linker, respectively. To achieve maximum %S of semi-IPN (588%) and IPN (500%), different parameters were optimized. The formation of cross-linked hydrogels and hydrogel composites with AgNPs was successfully demonstrated using FTIR analysis. The SEM investigation of hydrogel networks reveals a variety of morphologies, which could be attributed to structural differences between semi-IPN, IPN, and their composites with AgNPs. Semi-IPN, IPN and their composite showed superb antibacterial potential against *E. coli, M. luteus, P. aeruginosa, Rihzobium species, and S. aureus*, and may be used to treat a variety of infected effluents. Such interconnected hydrogels will give superior material properties, particularly in biomedical research, to prevent biomaterial-associated infections as well as general pathogenic invasions into the body. The synthesized hydrogel samples will lead to enhanced applications in the future, as well as a deeper knowledge of material interactions. The efforts to improve the property profile of cross-linked hydrogels are still on, with the hope of improving overall performance in terms of water uptake capacity, biocompatibility, and biodegradability.

Acknowledgements One of the authors Kashma Sharma is thankful to the University Grant Commission (UGC), New Delhi, India, for support through Post-Doctoral Fellowship for Women [F.15-1/2017/PDFWM-2017-18-HIM-51703(SA-II).

Authors' contributions The manuscript was written with contributions from all authors. All authors have approved the final version of the manuscript.

Declarations

Conflicts of interest The authors declare that they have no known competing financial interests or personal relationships that could have appeared to influence the work reported in this article.

References

1. Abasalizadeh F, Moghaddam SV, Alizadeh E et al (2020) Alginate-based hydrogels as drug delivery vehicles in cancer treatment and their applications in wound dressing and 3D bioprinting. J Biol Eng 14:8
2. Ahmed EM (2015) Hydrogel: Preparation, characterization, and applications: A review. J Adv Res 6:105–121
3. Zhu TX, Mao JJ, Cheng Y, Liu HR, Lv L, Ge MZ, Li SH, Huang JY, Chen Z, Li HQ, Yang L, Lai YK (2019) Recent progress of polysaccharide-based hydrogel interfaces for wound healing and tissue engineering. Adv Mater Interfaces 6:1900761
4. Kang G, Seong B, Gim Y, Lee H, Ko HS, Byun D (2019) Adv Mater Interfaces 6:1801885
5. Xiong R, Grant AM, Ma RL, Zhang SD, Tsukruk VV (2018) Mater Sci Eng R 125:1
6. Duan JJ, Liang XC, Zhu KK, Guo JH, Zhang LN (2017) Soft Matter 13:345
7. Bashir S, Hina M, Iqbal J, Rajpar AH, Mujtaba MA, Alghamdi NA, Wageh S, Ramesh K, Ramesh S (2020) Fundamental concepts of hydrogels: Synthesis, properties, and their applications. Polym 12:2702
8. Makhado E, Pandey S, Nomngongo PN et al (2018) Preparation and characterization of xanthan gum-cl-poly(acrylic acid)/o-MWCNTs hydrogel nanocomposite as highly effective re-usable adsorbent for removal of methylene blue from aqueous solutions. J Colloid Interf Sci 513:700–714
9. Malatji N, Makhado E, Modibane KD et al (2021) Removal of methylene blue from wastewater using hydrogel nanocomposites: A review. Nanomater Nanotechnol. https://doi.org/10.1177/18479804211039425
10. Lee KY, Mooney DJ (2012) Alginate: properties and biomedical applications. Prog Polym Sci 37:106–126
11. Zoratto N, Matricardi P (2018) Semi-IPN- and IPN-Based Hydrogels. In: Oliveira J, Pina S, Reis R, San Roman J (eds) Osteochondral Tissue Engineering. Advances in Experimental Medicine and Biology, vol 1059. Springer, Cham. https://doi.org/10.1007/978-3-319-76735-2_7
12. Kaur S, Jindal R (2018) Synthesis of interpenetrating network hydrogel from (Gum Copal alcohols-collagen)-co-poly(acrylamide) and acrylic acid: Isotherms and Kinetics study for removal of methylene blue dye from aqueous solution. Mater Chem Phys 220:75–86
13. Sukriti KBS, Jindal R (2017) Controlled biofertilizer release kinetics and moisture retention in gum xanthan-based IPN. Iran Polym J 26:563–577
14. Dai Z, Yang X, Feilun Wu, Wang L, Xiang K, Li P, Lv Q, Tang J, Dohlman A, Dai L, Shen X, You L (2021) Living fabrication of functional semi-interpenetrating polymeric materials. Nat Commun 12:3422
15. Pérez-Álvarez L, Ruiz-Rubio L, Lizundia E, Vilas-Vilela JL (2019) Polysaccharide-based superabsorbents: synthesis, properties, and applications. In: Mondal M (eds) Cellulose-Based Superabsorbent Hydrogels. Polymers and Polymeric Composites: A Reference Series. Springer, Cham. https://doi.org/10.1007/978-3-319-77830-3_46

16. Khan M, Shah LA, Rehman T, Khan A, Iqbal A, Ullah M, Alam S (2020) Synthesis of physically cross-linked gum Arabic-based polymer hydrogels with enhanced mechanical, load bearing and shape memory behavior. Iran Polym J 29:351–360
17. Sharma V, Arora N, Kumar R, Singh S, Verma S (2021) Effect of polyvinyl alcohol on electrical, spectroscopic and thermal properties of gum acacia-based gel electrolytes containing NaOH. Polym Bull. https://doi.org/10.1007/s00289-021-03915-3
18. Aderibigbe BA, Ray SS (2017) Gum acacia polysaccharide-based pH sensitive gels for targeted delivery of neridronate. Polym Bull 74:2641–2655
19. Ali BH, Ziada A, Blunden G (2009) Biological effects of gum arabic: a review of some recent research. Food Chem Toxicol 47:1–8
20. Juby KA, Dwivedi C, Kumar M, Kota S, Misra HS, Bajaj PN (2012) Silver nanoparticle-loaded PVA/gum acacia hydrogel: Synthesis, characterization and antibacterial study. Carbohyd Polym 89:906–913
21. Patel S, Goyal A (2015) Applications of natural polymer gum arabic: a review. Int J Food Propert 18:986–998
22. Behravesh A, Shahrousvand M, Goudarzi A (2021) Poly(acrylic acid)/gum arabic/ZnO semi-IPN hydrogels: synthesis, characterization and their optimizations by response surface methodology. Iran Polym J 30:655–674
23. Abdel-Bary EM, Elbedwehy AM (2018) Graft copolymerization of polyacrylic acid onto Acacia gum using erythrosine–thiourea as a visible light photoinitiator: application for dye removal. Polym Bull 75:3325–3340
24. Aisida SO, Ugwu K, Akpa PA, Nwanya AC, Ejikeme PM, Botha S, Ahmad I, Maaza M, Ezema FI (2019) Biogenic synthesis and antibacterial activity of controlled silver nanoparticles using an extract of Gongronema Latifolium. Mater Chem Phys 237:121859
25. Ren Y-Y, Yang H, Wang T, Wang C (2019) Bio-synthesis of silver nanoparticles with antibacterial activity. Mater Chem Phys 235:121746
26. Spasojevic J, Radosavljevic A, Krstic J, Jovanovic D, Spasojevic V, Kalagasidis-Krušic M, Kacarevic-Popovic Z (2015) Dual responsive antibacterial Ag-poly(N-isopropylacrylamide/itaconic acid) hydrogel nanocomposites synthesized by gamma irradiation. Eur Polym J 69:168–185
27. Krstic J, Spasojevic J, Radosavljevic A, Peric-Grujic A, Djuric M, Kacarevic-Popovic Z, Popovic S (2014) In vitro silver ion release kinetics from nanosilver/ poly(vinyl alcohol) hydrogels synthesized by gamma irradiation. J Appl Polym Sci 131:40321
28. Inbaneson S, Ravikumar S, Manikandan N (2011) Antibacterial potential of silver nanoparticles against isolated urinary tract infectious bacterial pathogens. Appl Nanosci 1:231–236
29. Vimala K, Sivudu KS, Mohan YM, Sreedhar B, Raju KM (2009) Controlled silver nanoparticles synthesis in semi-hydrogel networks of poly(acrylamide) and carbohydrates: a rational methodology for antibacterial application. Carbohyd Polym 75:463–471
30. Kora AJ, Sashidhar RB, Arunachalam J (2010) Gum kondagogu (Cochlospermum gossypium): A template for the green synthesis and stabilization of silver nanoparticles with antibacterial application. Carbohyd Polym 82:670–679
31. Zakia M, Koo JM, Kim D, Ji K, Huh PilHo, Yoon J, Yoo SI (2020) Development of silver nanoparticle-based hydrogel composites for antimicrobial activity. Green Chem Lett Rev 13(1):34–40. https://doi.org/10.1080/17518253.2020.1725149
32. Mohan YM, Vimala K, Thomas V, Varaprasad K, Sreedhar B, Bajpai SK, Raju KM (2010) Controlling of silver nanoparticles structure by hydrogel networks. J Colloid Interface Sci 342:73–82
33. Varaprasad K, Mohan YM, Ravindra S, Reddy NN, Vimala K, Monika K, Sreedhar B, Raju KM (2010) Hydrogel–silver nanoparticle composites: A new generation of antimicrobials. J Appl Polym Sci 115:1199–1207
34. Dai L, Nadeau B, An X, Cheng D, Long Z, Ni Y (2016) Silver nanoparticles-containing dual-function hydrogels based on a guar gum-sodium borohydride system. Sci Rep 6:36497. https://doi.org/10.1038/srep36497
35. Singh B, Dhiman A (2016) Design of Acacia gum–carbopol–cross-linked-polyvinylimidazole hydrogel wound dressings for antibiotic/anesthetic drug delivery. Ind Eng Chem Res 55:9176–9188
36. Li M, Li H, Li X, Zhu H, Xu Z, Liu L, Ma J, Zhang M (2017) A bioinspired alginate-gum arabic hydrogel with micro-/nanoscale structures for controlled drug release in chronic wound healing. ACS Appl Mater Interfaces 9:22160–22175
37. Singh B, Sharma S, Dhiman A (2017) Acacia gum polysaccharide based hydrogel wound dressings: Synthesis, characterization, drug delivery and biomedical properties. Carbohyd Polym 165:294–303
38. Bhatnagar M, Parwani L, Sharma V, Ganguli J, Bhatnagar A (2013) Hemostatic, antibacterial biopolymers from Acacia arabica (Lam.) Willd. and Moringa oleifera (Lam.) as potential wound dressing materials. Ind J Exp Bio 51:804–810
39. Sharma S, Virk K, Sharma K, Bose SK, Kumar V, Sharma V, Focarete ML, Kalia S (2020) Preparation of gum acacia-poly(acrylamide-IPN-acrylic acid) based nanocomposite hydrogels via polymerization methods for antimicrobial applications. J Mol Str 1215:128298
40. Magaldi S, Mata-Essayag S, Hartung de Capriles C, Perez C, Colella MT, Olaizola C, Ontiveros Y (2004) Well diffusion for antifungal susceptibility testing. Int J Infect Dis 8:39–45
41. Valgas C, Souza SM, Smânia EF, Smânia A Jr (2007) Screening methods to determine antibacterial activity of natural products. Braz J Microbiol 38:369–380
42. Rani P, Sen G, Mishra S, Jha U (2012) Microwave assisted synthesis of polyacrylamide grafted gum ghatti and its application as flocculant. Carbohyd Polym 89:275–281
43. Kaith BS, Ranjta S (2010) Synthesis of pH – Thermosensitive gum arabic based hydrogel and study of its salt-resistant swelling behavior for saline water treatment. Desalin Water Treat 24:28–37
44. He D, Susanto H, Ulbricht M (2009) Photo-irradiation for preparation, modification and stimulation of polymeric membranes. Prog Polym Sci 34:62–98
45. Zohuriaan-Mehr MJ, Motazedi Z, Kabiri K, Ershad-Langroudi A (2005) New super-absorbing hydrogel hybrids from gum arabic and acrylic monomers. J Macromol Sci Part A: Pure Appl Chem 42:1655–1666
46. Kabiri K, Zohuriaan-Mehr MJ (2004) Superabsorbent hydrogels from concentrated solution terpolymerization. Iran Polym J 13:423–430
47. Sharma K, Kaith BS, Kumar V, Kumar V, Som S, Kalia S, Swart HC (2013) Synthesis and properties of poly(acrylamide-aniline)-grafted Gum ghatti based nanospikes. RSC Adv 3:25830–25839
48. Kaith BS, Jindal R, Mittal H, Kumar K (2012) Synthesis, characterization, and swelling behavior evaluation of hydrogels based on gum ghatti and acrylamide for selective absorption of saline from different petroleum fraction–saline emulsions. J Appl Polym Sci 124:2037–2047
49. Pourjavadi A, Mahdavinia GR (2006) Superabsorbency, pH-sensitivity and swelling kinetics of partially hydrolyzed chitosan-g-poly(acrylamide) hydrogels. Turkish J Chem 30:595–608
50. Cheng Z, Li J, Yan J, Kang L, Ru X, Liu M (2013) Synthesis and properties of a novel superabsorbent polymer composite from microwave irradiated waste material cultured Auricularia auricula and poly (acrylic acid-co-acrylamide). J Appl Polym Sci 130:3674–3681
51. Fasiku VO, Aderibigbe BA, Sadiku ER, Lemmer Y, Owonubi SJ, Ray SS, Mukwevho E (2019) Polyethylene glycol–gum

acacia-based multidrug delivery system for controlled delivery of anticancer drugs. Polym Bull 76:5011–5037
52. Mbhele ZH, Salemane MG, van Sittert CGCE, Nedeljković JM, Djoković V, Luyt AS (2003) Fabrication and characterization of silver–polyvinyl alcohol nanocomposites. Chem Mater 15:5019–5024
53. Li Y, Sun ZZ, Rong JC, Xie B-B (2021) Comparative genomics reveals broad genetic diversity, extensive recombination and nascent ecological adaptation in Micrococcus luteus. BMC Genomics 22:124
54. Yang S, Sugawara S, Monodane T, Nishijima M, Adachi Y, Akashi S, Miyake K, Hase S, Takada H (2001) Micrococcus luteus Teichuronic Acids Activate Human and Murine Monocytic Cells in a CD14- and Toll-Like Receptor 4-Dependent Manner. Infect Immun 69:2025–2030
55. Feng Y, Mannion A, Madden CM, Swennes AG, Townes C, Byrd C, Marini RP, Fox JG (2017) Cytotoxic Escherichia coli strains encoding colibactin and cytotoxic necrotizing factor (CNF) colonize laboratory macaques. Gut Pathog 9:71
56. Lindström K, Mousavi SA (2019) Effectiveness of nitrogen fixation in rhizobia. Microb Biotechnol 13:1314–1335
57. Wu M, Li X (2015) Chapter 87 - Klebsiella pneumoniae and Pseudomonas aeruginosa. In: Tang YW, Sussman M, Liu D, Poxton I, Schwartzman J (eds) Molecular Medical Microbiology, (Second Edition), vol 3, Academic Press, pp 1547–1564. https://doi.org/10.1016/B978-0-12-397169-2.00087-1
58. Tong SYC, Davis JS, Eichenberger E, Holland TL, Fowler VG Jr (2015) Staphylococcus aureus infections: Epidemiology, pathophysiology, clinical manifestations, and management. Clin Microbiol Rev 28:603–661
59. Hu B, Owh C, Chee PL, Leow WR, Liu X, Wu Y-L, Guo P, Loh XJ, Chen X (2018) Supramolecular hydrogels for antimicrobial therapy. Chem Soc Rev 47:6917
60. Li S, Dong S, Xu W, Tu S, Yan L, Zhao C, Ding J, Chen X (2018) Antibacterial hydrogels. Adv Sci 5:1700527
61. Drlica K, Malik M, Kerns RJ, Zhao X (2008) Quinolone-mediated bacterial death. Antimicrob Agents Chemother 52:385–392
62. Vakulenko SB, Mobashery S (2003) Versatility of aminoglycosides and prospects for their future. Clin Microbiol Rev 16:430–450
63. Mohan YM, Vimal K, Thomas V, Varaprasad K, Sreedhar B, Bajpai SK, Raju KM (2010) Controlling of silver nanoparticles structure by hydrogel networks. J Colloid Interface Sci 342:73–82
64. Yan B, Mu Q, Jiang G, Chen L, Zhou H, Fourches D, Tropsha A (2014) Chemical basis of interactions between engineered nanoparticles and biological systems. Chem Rev 114:7740–7781
65. Morones JR, Elechiguerra JL, Camacho A, Holt K, Kouri JB, Ramirez JT, Yacaman MJ (2005) The bactericidal effect of silver nanoparticles. Nanotech 16:2346–2353
66. Sharma AK, Kaith BS, Shanker U, Gupta B (2020) γ-radiation induced synthesis of antibacterial silver nanocomposite scaffolds derived from natural gum Boswellia serrata. J Drug Deliv Sci Tech 56:101550
67. Dibrov P, Dzioba J, Gosink KK, Häse CC (2002) Chemiosmotic mechanism of antimicrobial activity of Ag+ in Vibrio cholera. Antimicrob Agents Chemother 46:2668–2670
68. Shukla AK, Alam J, Ansari MA, Alhoshan M, Alam M, Kaushik A (2019) Selective ion removal and antibacterial activity of silver-doped multi-walled carbon nanotube/ polyphenylsulfone nanocomposite membranes. Mater Chem Phy 233:102–112
69. Vellora Thekkae Padil V, Nguyen NH, Ševců A, Černík M (2015) Fabrication, characterization, and antibacterial properties of electrospun membrane composed of gum karaya, polyvinyl alcohol, and silver nanoparticles. J Nanomater 2015:10. Article ID 750726
70. Talodthaisong C, Boonta W, Thammawithan S, Patramanon R, Kamonsutthipaijit N, Hutchison JA, Kulchat S (2020) Composite guar gum-silver nanoparticle hydrogels as self-healing, injectable, and antibacterial biomaterials. Mater Today Commun 24:100992
71. Deka R, Sarma S, Patar P, Gogoi P, Sarmah JK (2020) Highly stable silver nanoparticles containing guar gum modified dual network hydrogel for catalytic and biomedical applications. Carbohydr Polym 248:116786
72. Yavari Maroufi L, Ghorbani M (2022) Development of a novel antibacterial hydrogel Scaffold based on guar gum/ooly (methylvinylether-alt-maleic Acid) containing cinnamaldehyde-loaded Chitosan nanoparticles. J Polym Environ 30:431–442
73. Ghaffari-Moghaddam M, Eslahi H (2014) Synthesis, characterization and antibacterial properties of a novel nanocomposite based on polyaniline/polyvinyl alcohol/Ag. Arab J Chem 7:846–855
74. Fadakar Sarkandi A, Montazer M, Harifi T, Mahmoudi Rad M (2021) Innovative preparation of bacterial cellulose/silver nanocomposite hydrogels: In situ green synthesis, characterization, and antibacterial properties. J Appl Polym Sci 138:e49824